

# Preparation of MOF-based Nitrogen Self-Doped Porous Carbon and Its Electrochemical Properties

Zhijian Zhang<sup>1</sup>, Pitao Wang<sup>2</sup>, Chi Zhang<sup>2</sup>, Shuai Li<sup>2</sup>, Jianqiang Zhang<sup>2,\*</sup>, and Heming Luo<sup>2,\*</sup>

<sup>1</sup> School of Material Science and Engineering, Lanzhou University of Technology, Lanzhou, 730050, P.R. China

<sup>2</sup> School of Petrochemical Engineering, Lanzhou University of Technology, Lanzhou, 730050, P.R. China

\*E-mail: [luohm666@163.com](mailto:luohm666@163.com)

Received: 7 November 2020 / Accepted: 28 December 2020 / Published: 31 January 2021

Metal-organic frameworks (MOFs) are widely used as precursors to prepare porous carbon materials due to their highly ordered porous structure and large specific surface area. In this paper, a metal-organic framework  $\{[\text{Zn}(\text{1,4-BDC})_{0.5}(\text{3-NH}_2\text{-trz})]\cdot(\text{solvent})\}_n$  was prepared using a solvent method as a precursor to prepare nitrogen self-doped porous carbon ZAPC-T by a direct carbonization, and the effect of different carbonization temperatures on the microstructures, compositions, and electrochemical properties of the nitrogen self-doped porous carbon ZAPC-T samples was investigated. Results showed that the specific surface area of ZAPC-800 reached  $728.57 \text{ m}^2 \text{ g}^{-1}$  with nitrogen and oxygen contents of 19.09% and 5.93%, respectively. When the carbonization temperature was  $800 \text{ }^\circ\text{C}$ , the specific capacitance of ZAPC-800 was  $225.4 \text{ F g}^{-1}$  at a current density of  $1.0 \text{ A g}^{-1}$ , and after 5000 cycles, the capacitance retention was as high as 83.01% with constant current charging and discharging. The specific capacitance decay rate was only 21.2% when the current density was increased from  $1.0 \text{ A g}^{-1}$  to  $10.0 \text{ A g}^{-1}$ . Thus, nitrogen self-doped porous carbon ZAPC-800 showed excellent electrochemical properties and good cycling stability. This study provides useful experimental data for the preparation of MOF-based nitrogen self-doped porous carbons and their applications.

**Keywords:** supercapacitor; metal-organic frameworks; hydrothermal method; nitrogen self-doped porous carbon; electrochemical

## 1. INTRODUCTION

With the rapid development of the global economy, the demand for energy by human society keeps increasing, and traditional fossil energy sources cause environmental pollution. Thus, the research and development of new clean energy sources is imperative [1]. Among the many energy storage devices, supercapacitors with short charging time, environmental friendliness, high power density and

long cycling life have become a research hotspot and have been widely used in mobile electronic devices, automobiles and other applications [2-5].

It is well known that the electrochemical performance of supercapacitors is largely dependent on the electrode materials; therefore, the preparation of advanced electrode materials is crucial for the electrochemical performance of supercapacitors [3, 6]. Carbon is the most widely used electrode material for supercapacitors due to its large specific surface area, excellent electronic conductivity, and good chemical stability [7-10]. Many studies have shown that doping carbon with nitrogen can improve the electrical conductivity and electrolyte wettability, which can significantly improve the electrochemical performance of supercapacitors [11-12]. The lone pair of electrons on nitrogen atoms can act as carriers to increase the number of carriers and the electrical conductivity of the porous carbon material. An increase in nitrogen-containing groups on the surface of a material can improve its surface hydrophilicity and make the electrode material come into better contact with the electrolyte [13-14]; additionally, pseudocapacitance can be generated by the redox reactions of nitrogen-containing functional groups [11,15].

In recent years, metal-organic framework materials (MOFs) with high specific surface areas have been increasingly studied as a new type of porous material [16-19], and with their diverse chemical compositions and structures, high specific surface areas and potential redox sites, MOFs as precursors have promising applications in material synthesis [20-24]. Jeon J W et al [25] successfully synthesized IRMOF-3 using nitrogen-rich organic ligands as carbon precursors, thereby preparing a nitrogen-doped porous carbon material with a three-dimensional (3D) structure by a one-step carbonization at 950 °C. The specific capacitance of this material was 239 F g<sup>-1</sup> at a scan rate of 5 mV s<sup>-1</sup>. Jing et al. [26] designed and prepared ZIF-8@ZIF-67 crystals with core-shell structures by the seed-mediated growth method. After a thermal treatment of the ZIF-8@ZIF-67 crystals, a selective functionalized nanoporous hybrid carbon material with nitrogen-doped carbon (NC) as the core and highly graphitic carbon (GC) as the shell was obtained. The electrochemical data strongly showed that the nanoporous hybrid carbon material combined the advantages of NC and GC, and the specific capacitance was 270 F g<sup>-1</sup> at a current density of 2 A g<sup>-1</sup>. Zhang P et al. [27] prepared a series of ZIF-based porous carbon materials by a direct carbonization using ZIF-7 as a carbon precursor and glucose, ethylene glycol, glycerol and furfuryl alcohol as secondary carbon sources. ZIF-7/glucose complex-derived carbon-L-950 was used as the electrode material for supercapacitors, and the specific capacitance reached 228 F g<sup>-1</sup> at a current density of 0.1 A g<sup>-1</sup>, and the capacitance retention rate was still 94% after 5000 cycles of charge and discharge at 5 A g<sup>-1</sup>. Luo et al [28] synthesized {[Ag<sub>3</sub>(BTC)(IM)]·H<sub>2</sub>O}<sub>n</sub> by a hydrothermal method, and the electrochemical properties of the self-doped nitrogen porous carbon ABIC-T in the mixed electrolyte of KOH and ASS-4.0 were investigated by direct carbonization. Nitrogen self-doped porous carbon ABIC-750 had a spongy porous structure with a specific surface area of 602 m<sup>2</sup> g<sup>-1</sup>. The specific capacitance of ABIC-750 was 142.2 F g<sup>-1</sup> at a current density of 1.0 A g<sup>-1</sup>, and the capacitance retention rate was 91.05% after 5000 charge and discharge cycles. The nitrogen self-doped porous carbon ABIC-750 had a specific capacitance of 817.1 F g<sup>-1</sup> at a current density of 1.0 A g<sup>-1</sup> in the ASS-4.0 mixed electrolyte, with an energy density that was 5.75 times higher than that in 6 M KOH, and the redox reaction with the mixed electrolyte of sodium alizarin sulfonate produced a Faraday quasi-capacitor, which greatly

increased the energy density of the supercapacitor. The above work shows that MOF-derived nitrogen self-doped porous carbon materials show potential as an ideal electrode material for supercapacitors.

In this paper,  $\{[\text{Zn}(1,4\text{-BDC})_{0.5}(3\text{-NH}_2\text{-trz})]\text{-(solvent)}\}_n$  was prepared by a solvent method, which was used as a carbon precursor to prepare nitrogen self-doped porous carbon ZAPC-T by direct carbonization, and the effect of the carbonization temperature on the microstructure and electrochemical properties of nitrogen self-doped porous carbon material ZAPC-T was investigated. This study provides an experimental basis for the directed synthesis of MOF precursors, the controlled preparation of nitrogen self-doped porous carbon materials with high capacitance and good rate performance, and the development of EDLCs with high energy density and power density.

## 2. EXPERIMENTAL

### 2.1 Preparation of $\{[\text{Zn}(1,4\text{-BDC})_{0.5}(3\text{-NH}_2\text{-trz})]\text{-(solvent)}\}_n$

Terephthalic acid (0.3735 g), 3-amino-1,2,4-triazole (0.0756 g), and zinc nitrate hexahydrate (0.5355 g) were dissolved in a mixture of 45 mL of DMF and 18 mL of H<sub>2</sub>O. This mixture was then placed in a 100 mL Teflon-lined stainless steel autoclave and heated to 100 °C for 72 h in a constant temperature oven. After cooling to room temperature, the white crystals ( $\{[\text{Zn}(1,4\text{-BDC})_{0.5}(3\text{-NH}_2\text{-trz})]\text{-(solvent)}\}_n$ ), abbreviated as ZAP, were obtained by filtrating three times with a mixture of deionized water and DMF and then drying under vacuum at 60 °C for 12 h.

### 2.2 Preparation of Nitrogen Self-Doped Porous Carbon ZAPC-T

ZAP was placed in a tube furnace with an argon atmosphere and heated to 700 °C, 750 °C, 800 °C and 850 °C at a heating rate of 3 °C min<sup>-1</sup>, and then kept at a constant temperature for 2 h. After natural cooling, the carbonized material was obtained. The carbonized material was immersed in 10% hydrochloric acid, washed with deionized water, filtered and dried to obtain nitrogen self-doped porous carbon, referred to as ZAPC-T (where C is for the nitrogen self-doped porous carbon and T is for the charring temperature).

### 2.3 Structural characteristics

The topography of the porous carbon material was observed using field emission scanning electron microscopy (SEM) (S-4800, Nippon Optical Corporation) and high-resolution transmission electron microscopy (JEOL JEM-2010, Nippon Optical Corporation). X-ray photoelectron spectroscopy (XPS) was also conducted (ESCALAB 250Xi, Seymour Fisher Scientific). Raman spectra were recorded by a 50 mW He-Ne laser operated at 633 nm by a Renishaw 1000 system using a CCD detector. Specific surface area, pore size distribution and total pore volume were measured using an ASAP 2020 instrument (Mike Instruments Inc., USA). XRD spectra were measured by an X'Pert Pro MPD X-ray diffractometer

(The Netherlands Panakot) with a Cu K $\alpha$ /graphite monochromator,  $\lambda = 0.1541$  nm, and a scanning speed of 10°/min with a scan range of 10°~90°.

#### 2.4 Working electrode

The mass ratio of ZAP, acetylene black and polytetrafluoroethylene (PTFE) was 80:15:5. This mixture was homogeneously dispersed in 20 mL of anhydrous ethanol, and the resulting slurry was coated on nickel foam (1 cm<sup>2</sup>) as electrodes. The active mass of each electrode sheet was between 3.0 and 5.0 mg. The electrode sheets were dried in vacuum at 80 °C for 24 h and pressed at 15 MPa for approximately 1.5 min.

#### 2.5 Electrochemical performance testing

This paper used a three-electrode system for electrochemical performance testing. A 6 M KOH solution was used as the electrolyte, ZAPC-T was used as the working electrode, a calomel electrode was used as the reference electrode, a platinum electrode was used as the counter electrode, and the voltage range was -1.0-0 V. The electrochemical performance measurements were obtained with cyclic voltammetry (CV), constant-current charge–discharge (GCD), and alternating current impedance (EIS) on a CHI660D electrochemical workstation manufactured by the Shanghai Chenhua company.

The specific capacitance  $C$  (F g<sup>-1</sup>) based on the constant current charge/discharge curve is calculated by Eq. (2.1):

$$C = \frac{I \cdot \Delta t}{m \cdot \Delta V} \quad (2.1)$$

where  $C$  is the specific capacitance of the carbon material (F g<sup>-1</sup>),  $I$  represents the discharge current (A),  $\Delta t$  is the discharge time corresponding to the voltage difference (s),  $m$  is the mass of active material in the electrode material (g), and  $\Delta V$  is the voltage change in the discharge time (V).

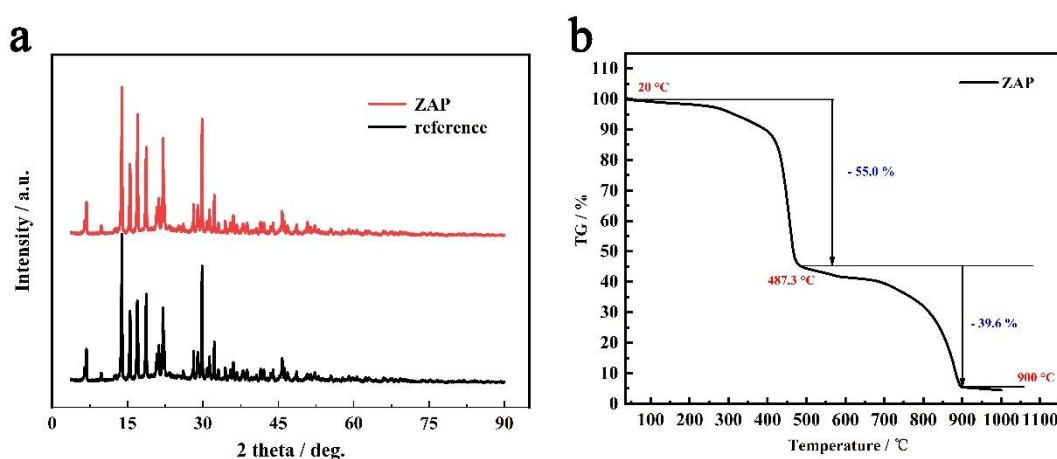
### 3. RESULTS AND DISCUSSION

#### 3.1 Physical analysis

##### 3.1.1 XRD and TGA analysis of ZAP

The powder X-ray diffraction pattern of ZAP is shown in Figure 1a. Sharp diffraction peaks at 6.82°, 13.84°, 15.5°, 18.7°, 22.08°, 29.82° and 32.24° were present, indicating that the prepared ZAP had good crystallinity. Among them, 13.84° and 29.82° were the characteristic diffraction peaks of ZAP, and the locations of these characteristic diffraction peaks were consistent with those reported in the literature [29]. The thermogravimetric analysis (Figure 1b) showed that the weight loss of ZAP was mainly divided into two stages: the first stage was from 25 °C to 487.3 °C, and there was an approximately 50% weight loss in this temperature range. The main cause of weight loss was the

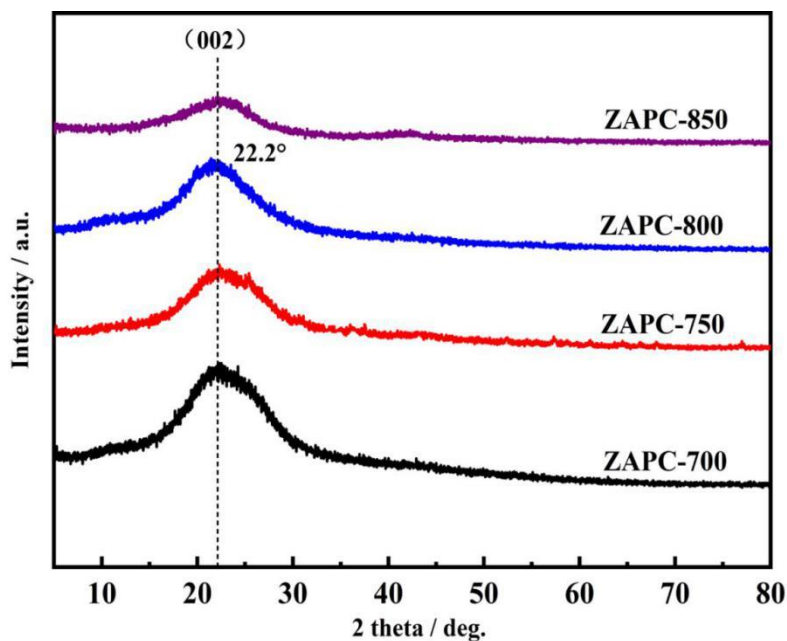
evaporation of water molecules and DMF adsorbed on the surface of the material when the temperature was lower than 200 °C. In the range of 200 °C ~ 487.3 °C, as the temperature continued to increase, part of the unstable ZAP skeleton collapsed, and a large number of water molecules, carbon dioxide and other gases escaped from the breaking of the carbon chain, which accelerated the weight loss phenomenon. The second stage was from 487.3 °C to 1000 °C, and the weight loss was approximately 36.9% in this temperature range. The main reasons for weight loss were as follows: at pyrolysis temperatures above 600 °C, the ZAP skeleton largely collapsed, and the carbon chain broke, producing ZnO, water molecules, carbon dioxide and other gases. As the temperature increased, ZnO and carbon produced zinc and CO<sub>2</sub> at temperatures above 800 °C. At 900 °C, gaseous Zn escaped with the nitrogen. This pyrolysis process revealed the pyrolytic changes of the ZAP skeleton, which provides an experimental basis for the preparation of highly porous carbon.



**Figure 1.** (a) XRD and (b) TGA results of ZAP

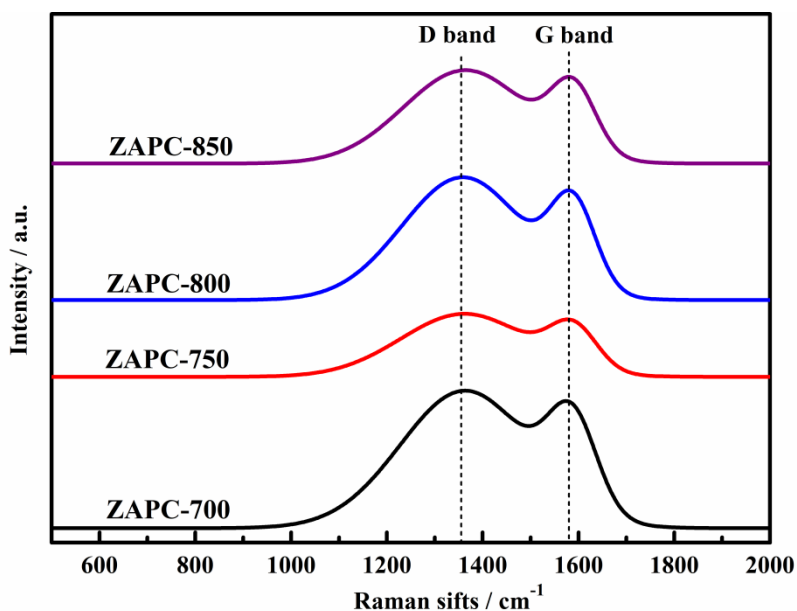
### 3.1.2 XRD analysis of the nitrogen self-doped porous carbon ZAPC-T

Figure 2 shows the X-ray diffraction pattern of nitrogen self-doped porous carbon ZAPC-T, from which it was observed that nitrogen self-doped porous carbon ZAPC-T had a characteristic diffraction peak at 22.2° corresponding to the (002) crystal surface of graphite, and a broad and dispersed diffraction peak at 22.2° for nitrogen self-doped porous carbon ZAPC-T; this diffraction peak significantly shifted to the left compared to that of standard graphite ( $2\theta \approx 26.6^\circ$ ). According to the Bragg's Law:  $2d \cdot \sin\theta = \lambda$ , the interlayer spacing between the (002) planes of graphite was increased, indicating that the graphitization of nitrogen self-doped porous carbon was low, which was due to the doping of nitrogen in the porous carbon material to form a large number of defects, so that carbon material lattice distortion occurred [30]. The doping of nitrogen improved the wettability of the carbon material and the electrolyte, which facilitated the migration of electrolyte ions into the interior of nitrogen self-doped porous carbon ZAPC-T and improved the electrochemical performance of nitrogen self-doped porous carbon ZAPC-T. No other heterogeneous peaks were observed in the XRD of ZAPC-T, and the metals and their compounds could be removed in the pickling process of the carbon material, and the XRD results were consistent with the TGA results.



**Figure 2.** X-ray diffraction patterns of the self-doped nitrogen porous carbon ZAPC-T samples

### 3.1.3 Raman analysis of nitrogen self-doped porous carbon ZAPC-T



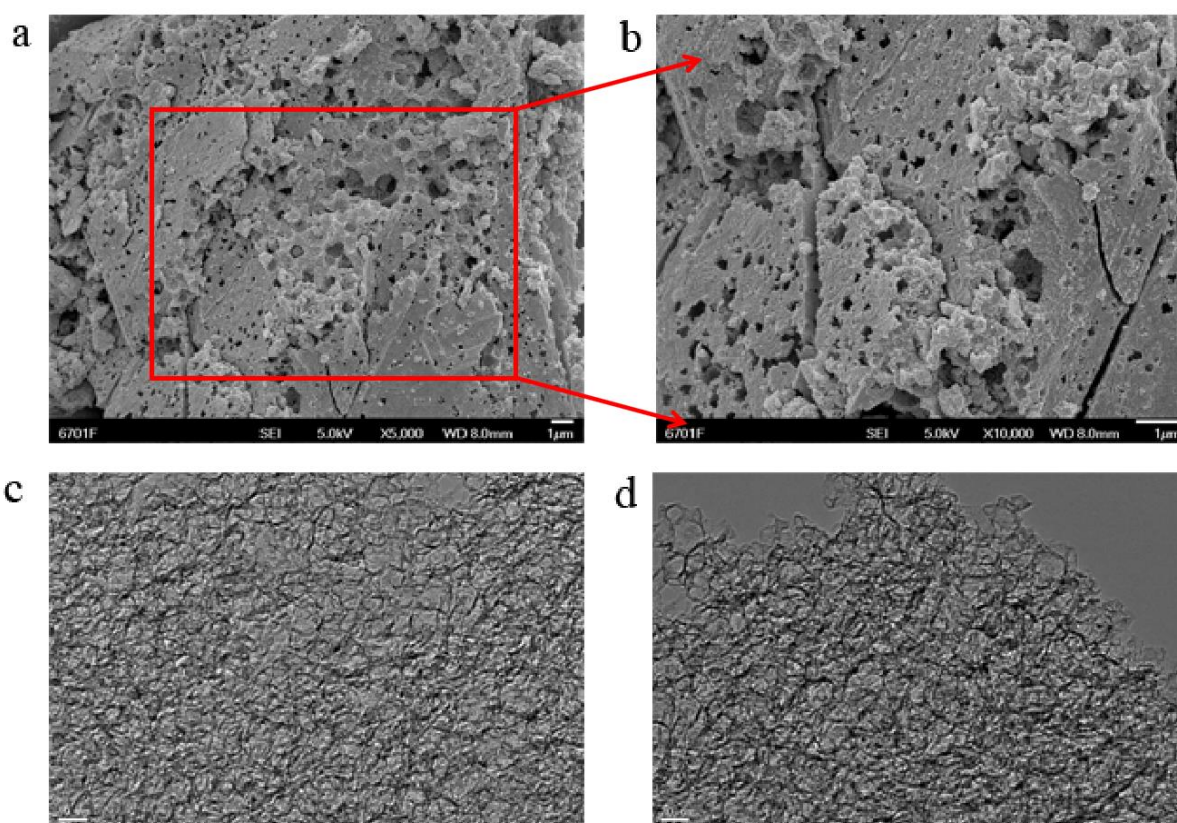
**Figure 3.** Raman spectra of nitrogen self-doped porous carbon ZAPC-T

Figure 3 shows the Raman spectra of the nitrogen self-doped porous carbon ZAPC-T samples, all of which have two distinctive peaks: the D band at  $1355\text{ cm}^{-1}$  (disordered carbon or defective graphite structure) and the G band at  $1580\text{ cm}^{-1}$  (graphite structure of  $\text{sp}^2$  hybridized carbon atoms). The intensity ratio ( $I_D/I_G$ ) of the G and D-bands is widely used to evaluate the graphitization of carbon materials [31]. As shown in Figure 3, the  $I_D/I_G$  values of nitrogen self-doped porous carbon were 1.435 (ZAPC-700),

1.426 (ZAPC-750), 1.402 (ZAPC-800) and 1.323 (ZAPC-850). With increasing charring temperature, the nitrogen self-doped porous carbon ZAPC-T became less disordered, and the graphitization increased, which facilitated the charge transfer of nitrogen self-doped porous carbon ZAPC-T, thus improving its electrochemical properties. The stronger D-peak in the Raman spectrum proved that the material had lower graphitization and more defects, which were mainly caused by nitrogen doping, which disrupted the charge balance of the carbon atoms to produce defect sites. Heteroatom doping contributed to the improvement of the electrochemical properties of materials [32]. Thus, Raman spectroscopy indirectly proved that the nitrogen self-doped porous carbon ZYC-T was an amorphous carbon.

### 3.2 Microstructure

#### 3.2.1 Morphological analysis



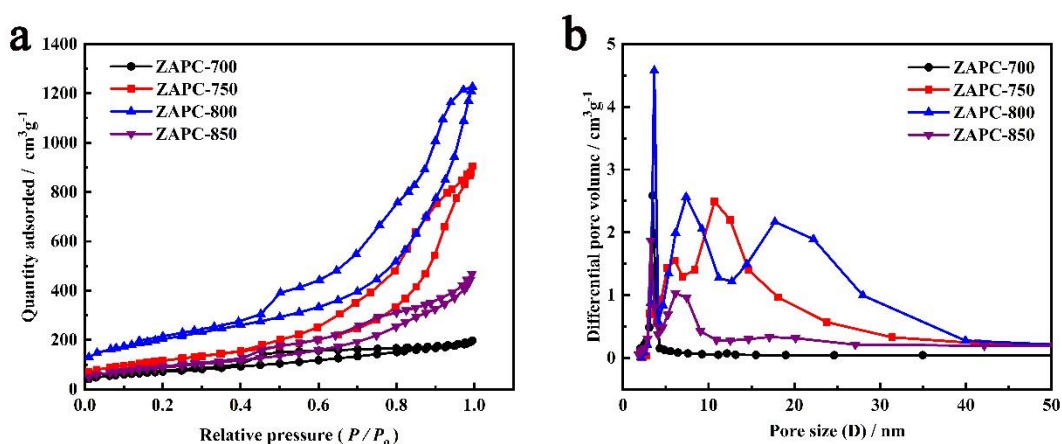
**Figure 4.** (a, b) SEM images and (c, d) TEM images of nitrogen self-doped porous carbon ZAPC-800

Figure 4 shows the scanning electron microscopy and transmission electron microscopy analysis of the nitrogen self-doped porous carbon ZAPC-800, as shown in Figure 4 (a, b). The porous structure of nitrogen self-doped porous carbon ZAPC-800 consisted of micropores, mesopores and macropores, and the various pore sizes were conducive to the fast transfer of electrolyte ions to the electrode active phase, thus promoting the electrochemical reaction. In addition, some of the observed macroporous channels were composed of stacked loose carbon material particles. From the transmission electron

microscopy images in Figure 4 (c, d), it can be observed that nitrogen self-doped porous carbon ZAsPC-800 had an abundance of meandering snake-shaped pore channels, which further indicated that nitrogen self-doped porous carbon ZAPC-800 had an abundant pore structure, and in addition, nitrogen self-doped porous carbon ZAPC-800 exhibited a disordered lattice structure, indicating that the nitrogen self-doped porous carbon ZAPC-800 had an amorphous graphite structure.

### 3.2.2 $N_2$ adsorption/desorption

Figure 5 shows the nitrogen adsorption/desorption curves and pore size distribution curves of ZAPC-T. As shown in Figure 5a, all samples exhibited similar type IV adsorption/desorption curves at relatively low pressure ( $<0.01$ ) [33], and it could be observed that the  $N_2$  adsorption/desorption curves showed an increasing trend at a relative pressure  $P/P_0$  close to 0, indicating that a certain number of micropores existed in the nitrogen self-doped porous carbon ZAPC-T. When the relative pressure was increased to 0.4-0.85, an H3-type “hysteresis loop” appeared, which indicated that there were an abundance of mesoporous structures in ZAPC-T. When the relative pressure was increased to nearly 1.0, the  $N_2$  adsorption capacity of ZAPC-T increased significantly, which indicated that ZAPC-T contained macropores. The mesopores and macropores could promote the diffusion of electrolyte ions into the electrode, and the micropores increased the effective utilized area of carbon material and improved the electrochemical performance of ZAPC-T.



**Figure 5.** (a)  $N_2$  adsorption/desorption curves and (b) pore size distribution curves of the nitrogen self-doped porous carbon ZAPC-T samples

The pore size distribution curves of the nitrogen self-doped porous carbon ZAPC-T were calculated by density functional theory (DFT), as shown in Figure 5b, and most of the pore size distribution of the nitrogen self-doped porous carbon ZAPC-T was located in the mesopore region. Combined with Table 1, the average pore sizes of ZAPC-700, ZAPC-750, ZAPC-800 and ZAPC-850 were 4.36 nm, 12.17 nm, 9.25 nm and 7.70 nm, respectively, indicating that the nitrogen self-doped porous carbon ZAPC-T had a diversified pore size distribution. The specific surface areas of nitrogen-doped porous carbon ZAPC-T were  $258.87 \text{ m}^2 \text{ g}^{-1}$ ,  $421.87 \text{ m}^2 \text{ g}^{-1}$ ,  $728.57 \text{ m}^2 \text{ g}^{-1}$  and  $324.21 \text{ m}^2 \text{ g}^{-1}$ , and

the pore volumes were  $0.28 \text{ cm}^3 \text{ g}^{-1}$ ,  $1.28 \text{ cm}^3 \text{ g}^{-1}$ ,  $1.68 \text{ cm}^3 \text{ g}^{-1}$  and  $0.62 \text{ cm}^3 \text{ g}^{-1}$ , respectively, which showed a tendency of increasing and then decreasing in regard to the Brunauer-Emmett-Teller (BET) specific surface areas and pore volumes. Due to the pyrolysis process, some of the micropores and mesopores gradually developed into mesopores and macropores with increasing temperature. The above results indicated that the charring temperature was critical for the evolution of the carbon material microstructure.

**Table 1.** Specific surface areas and parameter characteristics of the nitrogen self-doped porous carbon ZAPC-T samples

Materials	$S_{\text{BET}}$ ( $\text{m}^2 \text{ g}^{-1}$ )	$V_{\text{total}}$ ( $\text{cm}^3 \text{ g}^{-1}$ )	$D_{\text{average}}$ (nm)
ZAPC-700	258.87	0.28	4.36
ZAPC-750	421.87	1.28	12.17
ZAPC-800	728.57	1.68	9.25
ZAPC-850	324.21	0.62	7.70

### 3.3 Surface composition analysis

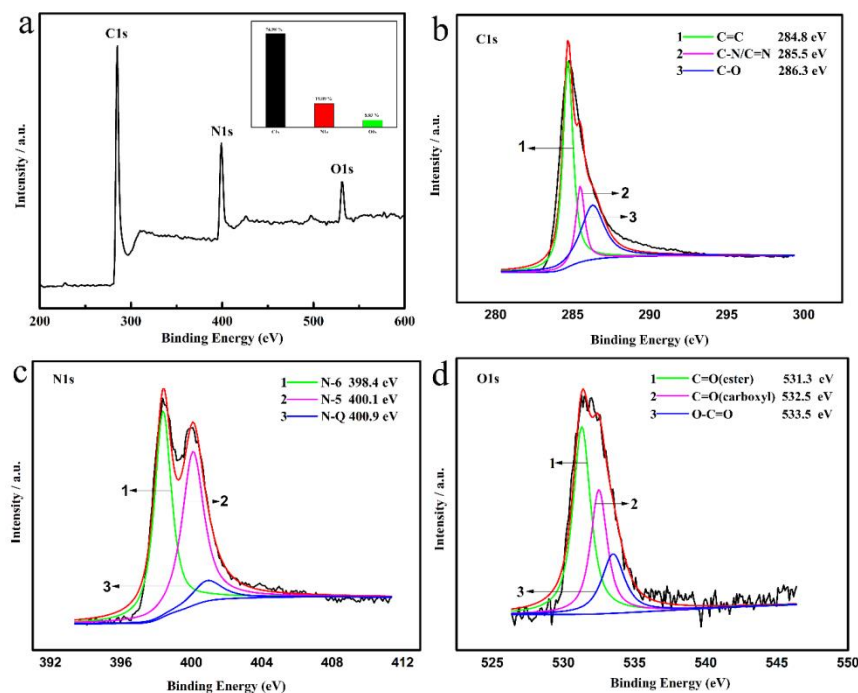


**Figure 6.** XPS spectrum of nitrogen self-doped porous carbon ZAPC-800: (a) XPS full spectrum, (b) C 1s, (c) N 1s, and (d) O 1s

To further determine the chemical composition and bonding mode of nitrogen self-doped porous carbon ZAPC-800, X-ray photoelectron spectroscopy (XPS) was carried out, as shown in Figure 6a, which showed that nitrogen self-doped porous carbon ZAPC-800 was composed of carbon, nitrogen and oxygen with contents of 74.98%, 19.09% and 5.93%, respectively. The spectra showed the existence of three characteristic peaks at 285.1 eV, 399.2 eV, and 531.3 eV, corresponding to C 1s, N 1s, and O 1s [34-35]. As shown in Figure 6b, the XPS spectra of C 1s revealed three forms of carbon: C=C, C-N/C=N, and C-O at 284.8 eV, 285.5 eV, and 286.3 eV, respectively [36], accounting for 47.43%, 14.01%, and 38.56%, respectively (Table 2). Moreover, the presence of C-N/C=N contributed to the pseudocapacitance, which helped to enhance the electrochemical properties. As shown in Figure 6c, the XPS spectra of the N 1s revealed the presence of three forms of nitrogen: pyridinic nitrogen (N-6) at 398.4 eV, pyrrolic nitrogen (N-5) at 400.1 eV and graphitic nitrogen (N-Q) at 400.9 eV [37], and the proportions of N-6, N-5 and N-Q in the surface nitrogen functional groups were 42.80%, 39.55% and 17.65% (Table 2), respectively. The results show that the dominant pyrrolic and pyridinic nitrogen were the main factors that led to the Faraday effect in the electrode material, while the presence of graphitic nitrogen could improve the electrical conductivity of the carbon material; therefore, these factors improved the rate performance and cycling stability of the carbon material. As shown in Figure 6d, the characteristic peaks of the O 1s spectrum at 531.3 eV, 532.5 eV and 533.5 eV represented C=O(ester), C=O(carboxyl) and O-C=O [38, 39], respectively. Among the surface oxygen functional groups, C=O (ester), C=O (carboxyl), and O-C=O accounted for 53.75%, 30.23%, and 16.02%, respectively (Table 2). Among them, C=O (ester) and C=O (carboxyl) dominated.

**Table 2.** XPS analysis data of nitrogen self-doped porous carbon ZAPC-800

Element	Bind Energy (eV)	Content (at%)
C 1s	284.8	47.43
	285.5	14.01
	286.3	38.56
N 1s	398.4	42.80
	400.1	39.55
	400.9	17.65
O 1s	531.3	53.75
	532.5	30.23
	533.5	16.02

### 3.4 Electrochemical properties

#### 3.4.1 Electrochemical properties of nitrogen self-doped porous carbon ZAPC-T

Figure 7 shows the electrochemical performance test of nitrogen self-doped porous carbon ZAPC-T. As shown in Figure 7a, all the curves of ZAPC-T were asymmetric isosceles triangles, indicating the existence of pseudocapacitance in addition to the double layer capacitance of ZAPC. The

pseudocapacitance was caused by the redox reaction of pyrrolic nitrogen and pyridinic nitrogen in the nitrogen self-doped porous carbon. As shown in Figure 7b, the specific capacitance of ZAPC-700, ZAPC-750, ZAPC-800 and ZAPC-850 reached  $166.2 \text{ F g}^{-1}$ ,  $204.2 \text{ F g}^{-1}$ ,  $225.4 \text{ F g}^{-1}$  and  $177.6 \text{ F g}^{-1}$ , respectively, at  $1.0 \text{ A g}^{-1}$ [40]. With the increase in the carbonization temperature, the specific capacitance of the nitrogen self-substituted porous carbon ZAPC-T first showed an increase and then decreased. The main reason for this result was that a high carbonization temperature was beneficial to the formation of pores, but a carbonization temperature that was too high would collapse the pore structure, resulting in a decreased specific surface area and a decreased electrochemical performance. When the current density increased from  $1.0 \text{ A g}^{-1}$  to  $10.0 \text{ A g}^{-1}$ , the specific capacitance of the nitrogen self-doped porous carbon ZAPC-T decreased, and the nitrogen self-doped porous carbon ZAPC-700, ZAPC-750, ZAPC-800 and ZAPC-850 capacitance attenuation rates were 24.1%, 24.3%, 21.2% and 23.6%, respectively.

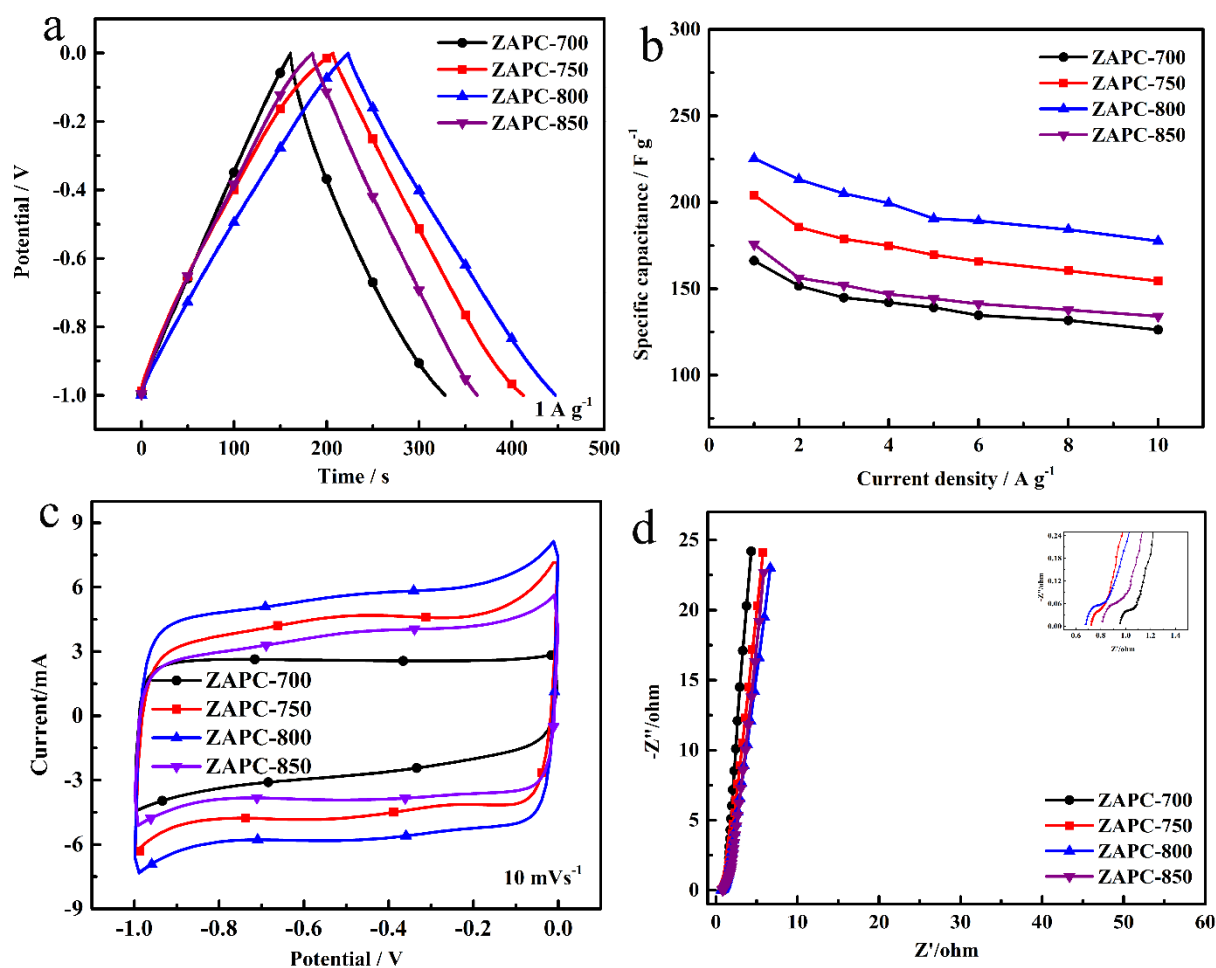


**Figure 7.** Electrochemical performance test of the nitrogen self-doped porous carbon ZAPC-T samples: (a) GCD curves at  $1.0 \text{ A g}^{-1}$ , (b) specific capacitances calculated based on GCD, (c) CV curves at  $10 \text{ mV s}^{-1}$ , and (d) Nyquist plots

The attenuation of the specific capacitance was mainly because the electrolyte ions could better enter the active sites of the electrode at a low current density, which increased the utilization rate of the material. At high current density, the electron transfer rate increased, and the ions or electrons

participating in the electrochemical reaction did not have sufficient time to transfer, resulting in a decrease in the specific capacitance and a decrease in the rate charge-discharge performance[41]. As shown in Figure 7c, the CV curve showed that the nitrogen self-doped porous carbon ZAPC-T exhibited a similar rectangular shape, indicating that the nitrogen self-doped porous carbon ZAPC-T exhibited both electric double-layer capacitive behaviour and more obvious pseudocapacitive behaviour. This result was due to the presence of nitrogen and oxygen functional groups in the nitrogen self-doped porous carbon ZAPC-T, resulting in a weak redox peak in the CV curve, which also fully demonstrated the effective combination of the double-layer capacitive and pseudocapacitive performance. The electrochemical impedance of nitrogen self-doped porous carbon ZAPC-T is shown in Figure 7d, and the Nyquist plots of all the nitrogen self-doped porous carbon ZAPC-T samples were almost perpendicular to the real axis in the low frequency region, indicating that the nitrogen self-doped porous carbon ZAPC-T had good capacitive behaviour[42]. In the high-frequency region, the intercept between the Nyquist plot and the real axis was the alternating current series resistance (ESR), in which the alternating current series resistance (ESR) values of ZAPC-700, ZAPC-750, ZAPC-800 and ZAPC-850 were 0.956 $\Omega$ , 0.722 $\Omega$ , 0.680 $\Omega$  and 0.814 $\Omega$ , respectively. The low impedance of ZAPC-T revealed that the material had good electrical conductivity and charge transport properties. Among them, the nitrogen self-doped porous carbon ZAPC-800 had the lowest equivalent series resistance, which was consistent with its excellent electrochemical properties.

#### 3.4.2 Electrochemical Properties of Nitrogen Self-Doped Porous Carbon ZAPC-800

Figure 8 shows the electrochemical test of nitrogen self-doped porous carbon ZAPC-800. Figure 8a shows the constant current charge and discharge curves of nitrogen-doped porous carbon ZAPC-800 at different current densities. It can be seen from the figure that the charge and discharge curves at different current densities were isosceles triangles, which exhibited obvious double electric layer capacitive behaviour[43]. As shown in Figure 8b, the nitrogen self-doped porous carbon ZAPC-800 capacitor decayed from 225.4 F g<sup>-1</sup> to 177.6 F g<sup>-1</sup> when the current density was increased from 1.0 A g<sup>-1</sup> to 10.0 A g<sup>-1</sup>, with a decay rate of only 21.2%. The good rate charge-discharge performance of the nitrogen self-doped porous carbon ZAPC-800 was attributed to its good electrical conductivity and very porous structure. As shown in Figure 8c, the CV curves of ZAPC-800 showed a similar rectangular shape at different scan rates, indicating that the nitrogen self-doped porous carbon ZAPC-800 exhibited both electric double-layer capacitive and pseudocapacitance behaviour. As shown in Figure 8d, the capacitance retention rate of nitrogen self-doped porous carbon ZAPC-800 was still 83.01% after 5000 cycles of constant current charge and discharge at a current density of 1.0 A g<sup>-1</sup>. The reason for the decrease in capacitance retention rate might be that nitrogen self-doped porous carbon ZAPC-800 showed partial functional group damage or decreased capacitance retention due to electrolyte ion buildup within the material as the number charge-discharge cycles increased. The higher capacitance retention of the nitrogen self-doped porous carbon ZAPC-800 showed its good cycling stability.

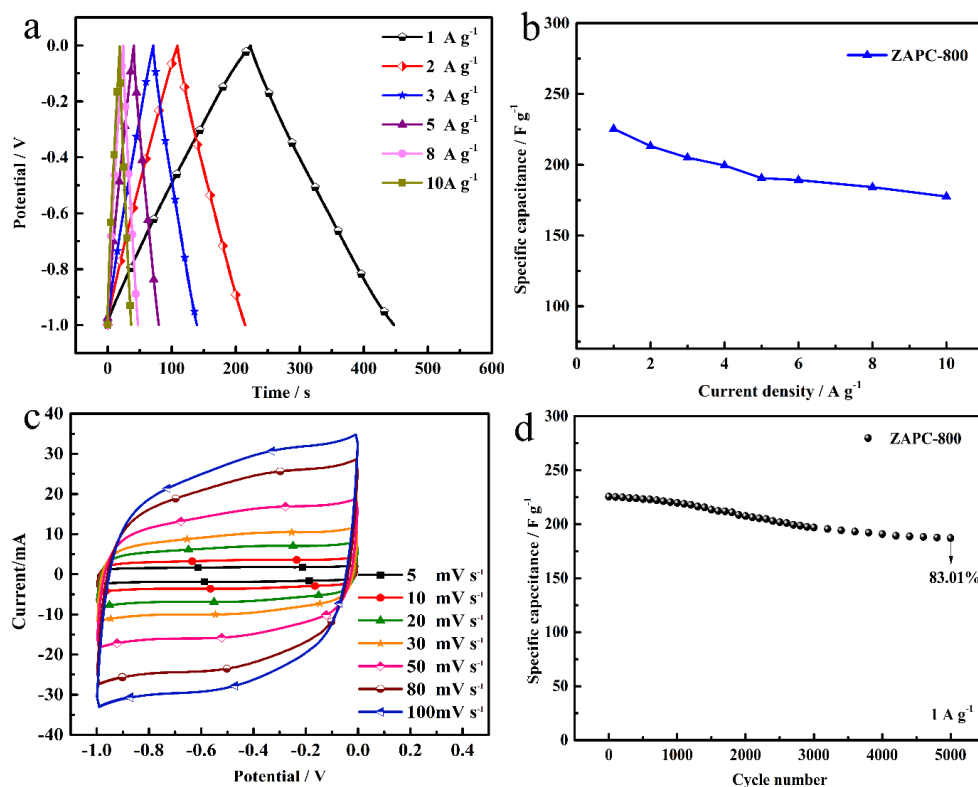


**Figure 8.** Electrochemical test of nitrogen self-doped porous carbon ZAPC-800: (a) GCD curves at different current densities, (b) specific capacitance based on GCD curves, (c) CV curves at different scan rates, and (D) cycling performance at a current density of 1.0 A g<sup>-1</sup>

#### 4. CONCLUSIONS

In this paper, ZAP was successfully prepared by a solvent method, and nitrogen self-doped porous carbon ZAPC-T was prepared by a direct carbonization using ZAP as a precursor. The results showed that the nitrogen self-doped porous carbon ZAPC-800 exhibited an amorphous graphitic carbon structure with mesopores, and the specific surface area of the carbon material was as high as 728.57 m<sup>2</sup> g<sup>-1</sup> with nitrogen and oxygen contents of 19.09% and 5.93%, respectively. Nitrogen self-doped porous carbon ZAPC-800 had a high specific capacitance of 225.4 F g<sup>-1</sup> at 1.0 A g<sup>-1</sup>, and the attenuation rate was only 14.18% when the current density increased from 1.0 A g<sup>-1</sup> to 10.0 A g<sup>-1</sup>. At a current density of 1.0 A g<sup>-1</sup>, the capacitance retention rate of ZAPC-800 was still 83.01% after 5000 cycles of charging and discharging, which showed the excellent electrochemical performance of ZAPC-800.

#### ACKNOWLEDGEMENTS

This work is partially supported by the fund of National Nature Science Foundation of China (Nos. 21667017 and 21666018) and the Gansu Province University Fundamental Research Funds (No. 056002).

## References

1. P. C. Stern, K. B. Janda, M. A. Brown, L. Steg, E. L. Vine and L. Lutzenhiser, *Nat. Energy*, 1 (2016) 1.
2. J. Chen, B. Luo, Q. Chen, F. Li, Y. Guo, T. Wu, P. Peng, X. Qin, G. Wu and M. Cui, *Adv. Mater.*, 32 (2020) e1905578.
3. J. Y. Seok, S. A. Song, I. Y. Yang, K. Woo, S. Y. Park, J. H. Park, S. Kim, S. S. Kim and M. Y. Yang, *Adv. Mater. Interfaces*, 7 (2020) e2000513.
4. L. L. Ma, M. Y. Jin, C. J. Yan, H. Guo and X. H. Ma, *Macromol. Mater. Eng.*, 305 (2020) e1900807.
5. F. Yu, T. Wang, Z. Wen and H. Wang, *J. Power Sources*, 364 (2017) 9.
6. Y. Jiang, X. Yan, Y. Cheng, Y. Zhang, W. Xiao, L. Gan and H. Tang, *RSC Adv.*, 9 (2019) 13207.
7. L. Wei, M. Sevilla, A. B. Fuertes, R. Mokaya and G. Yushin, *Adv. Energy Mater.*, 1 (2011) 356.
8. J. Y. Hwang, M. Li, M. F. El - Kady and R. B. Kaner, *Adv. Funct. Mater.*, 27 (2017) 1605745.
9. B. Kim, H. Chung and W. Kim, *J. Phys. Chem. C*, 114 (2010) 15223.
10. H. Li, Y. Tao, X. Y. Zheng, J. Y. Luo, F. Y. Kang, H. M. Cheng and Q. H. Yang, *Energy Environ. Sci.*, 9 (2016) 3135.
11. Z. W. Tian, M. Xiang, J. C. Zhou, L. Q. Hu and J. J. Cai, *Electrochim. Acta*, 211 (2016) 225.
12. W. J. Lu, S. Z. Huang, L. Miao, M. X. Liu, D. Z. Zhu, L. C. Li, H. Duan, Z. J. Xu and L. H. Gan, *Chin. Chem. Lett.*, 28 (2017) 1324.
13. T. Wang, Z. Dong, T. Fu, Y. C. Zhao, T. Wang, Y. Z. Wang, Y. Chen, B. H. Han and W. P. Ding, *Chem Commun.*, 51 (2015) 17712.
14. K. P. Gong, F. Du, Z. H. Xia, M. Durstock and L. M. Dai, *Science*, 323 (2009) 760.
15. S. Yu, D. Liu, S. Zhao, B. Bao, C. Jin, W. Huang, H. Chen and Z. Shen, *RSC Adv.*, 5 (2015) 30943.
16. A. Kirchon, L. Feng, H. F. Drake, E. A. Joseph and H. C. Zhou, *Chem. Soc. Rev.*, 47 (2018) 8611.
17. B. Y. Guan, X. Y. Yu, H. B. Wu and X. W. Lou, *Adv. Mater.*, 29 (2017) 1703614.
18. S. L. Yang, L. Peng, S. Bulut and W. L. Queen, *Chemistry*, 25 (2019) 2161.
19. T. Deng, Y. Lu, W. Zhang, M. L. Sui, X. Y. Shi, D. Wang and W. T. Zheng, *Adv. Energy Mater.*, 8 (2018) 1702294.
20. A. J. Han, B. Q. Wang, A. Kumar, Y. J. Qin, J. Jin, X. H. Wang, C. Yang, B. Dong, Y. Jia, J. F. Liu and X. M. Sun, *Small Methods*, 3 (2019) e1800471.
21. Y. F. Gu, Y. N. Wu, L. C. Li, W. Chen, F. T. Li and S. Kitagawa, *Angew. Chem., Int. Ed.*, 56 (2017) 15658.
22. G. Y. Xu, P. Nie, H. Dou, B. Ding, L. Y. Li and X. G. Zhang, *Mater. Today*, 20 (2017) 191.
23. P. Silva, S. M. F. Vilela, J. P. C. Tome and F. A. A. Paz, *Chem. Soc. Rev.*, 44 (2015) 6774.
24. K. Chen, Z. H. Sun, R. P. Fang, Y. Shi, H. M. Cheng and F. Li, *Adv. Funct. Mater.*, 28 (2018), 1707592.
25. J. W. Jeon, R. Sharma, P. Meduri, B. W. Arey, H. T. Schaefer, J. L. Lutkenhaus, J. P. Lemmon, P. K. Thallapally, M. I. Nandasiri, B. P. McGrail and S. K. Nune, *ACS Appl. Mater. Interfaces*, 6 (2014) 7214.
26. J. Tang, R. R. Salunkhe, J. Liu, N. L. Torad, M. Imura, S. Furukawa and Y. Yamauchi, *J. Am. Chem. Soc.*, 137 (2015) 1572.
27. P. Zhang, F. Sun, Z. G. Shen and D. P. Cao, *J. Mater. Chem. A*, 2 (2014) 12873.
28. Q. Wang, S. Li, J. Zhang, X. Zhao, H. Feng and H. Luo, *Appl. Surf. Sci.*, 500 (2020) e143936.
29. B. Liu, R. Zhao, G. Yang, L. Hou, Y.-Y. Wang and Q.-Z. Shi, *CrystEngComm*, 15 (2013) 2057.
30. Z. H. Li, M. F. Shao, L. Zhou, R. K. Zhang, C. Zhang, M. Wei, D. G. Evans and X. Duan, *Adv. Mater.*, 28 (2016) 2337.
31. L. Wei, M. Sevilla, A. B. Fuertes, R. Mokaya and G. Yushin, *Adv. Funct. Mater.*, 22 (2012) 827.
32. J. C. Zhang, J. S. Zhou, D. Wang, L. Hou and F. M. Gao, *Electrochim. Acta*, 191 (2016) 933.
33. H. T. Liu, Z. Q. Shan, W. L. Huang, D. D. Wang, Z. J. Lin, Z. J. Cao, P. Chen, S. X. Meng and L.

- Chen, *ACS Appl. Mater. Interfaces*, 10 (2018) 4715.
34. Li, Sun, Chungui, Tian, Yu, Fu, Ying, Yang, Jie and Yin, *Chem. - Eur. J.*, 20 (2013) 564.
  35. X. Kang, C. Wang and J. Yin, *ChemElectroChem*, 4 (2017) 2599.
  36. S. Huang, J. Zhang, P. Li, W. Wang, H. Feng and H. Luo, *Appl. Surf. Sci.*, 459 (2018) 120.
  37. Z. Zhang, L. Li, Y. Qing, X. Lu, Y. Wu, N. Yan and W. Yang, *J. Phys. Chem. C*, 122 (2018) 23852.
  38. P. Thirukumaran, R. Atchudan, A. Shakila Parveen, Y. R. Lee and S. C. Kim, *J. Alloys Compd.*, 750 (2018) 384.
  39. J.-J. Zhang, H.-X. Fan, X.-H. Dai and S.-J. Yuan, *R. Soc. Open Sci.*, 5 (2018) e172456.
  40. W. Xing, C. C. Huang, S. P. Zhuo, X. Yuan, G. Q. Wang, D. Hulicova-Jurcakova, Z. F. Yan and G. Q. Lu, *Carbon*, 47 (2009) 1715.
  41. H. S. Fan, H. Wang, N. Zhao, J. Xu and F. Pan, *Sci. Rep.*, 4 (2013) 7426.
  42. K. Wang, N. Zhao, S. Lei, R. Yan, X. Tian, J. Wang, Y. Song, D. Xu, Q. Guo and L. Liu, *Electrochim. Acta*, 166 (2015) 1.
  43. L. Lv, Y. Huang and D. Cao, *Appl. Surf. Sci.*, 456 (2018) 184.

© 2021 The Authors. Published by ESG ([www.electrochemsci.org](http://www.electrochemsci.org)). This article is an open access article distributed under the terms and conditions of the Creative Commons Attribution license (<http://creativecommons.org/licenses/by/4.0/>).